Journal of Materials Chemistry A

PAPER

View Article Online
View Journal | View Issue

Cite this: J. Mater. Chem. A, 2014, 2, 8483

Improved lithium ion battery performance by mesoporous Co_3O_4 nanosheets grown on self-standing $NiSi_x$ nanowires on nickel foam†

Huixin Chen,‡[a] Qiaobao Zhang,‡[b] Jiexi Wang,[c] Daguo Xu,[b] Xinhai Li,[c] Yong Yang*[a] and Kaili Zhang*[b]

Received 25th February 2014
Accepted 24th March 2014

DOI: 10.1039/c4ta00967c

www.rsc.org/MaterialsA

Novel three-dimensional (3D) hierarchical $NiSi_x/Co_3O_4$ core–shell nanowire arrays composed of $NiSi_x$ nanowire cores and branched Co_3O_4 nanosheet shells have been successfully synthesized by combining chemical vapor deposition and a simple but effective chemical bath deposition process followed by a calcination process. The resulting hierarchical $NiSi_x/Co_3O_4$ core–shell nanowire arrays directly serve as binder- and conductive-agent-free electrodes for lithium ion batteries, which demonstrate remarkably improved electrochemical performances with excellent capacity retention and high rate capability on cycling. They can maintain a stable reversible capacity of 1279 mA h g^{-1} after 100 cycles at a current density of 400 mA g^{-1} and a capacity higher than 340 mA h g^{-1} even at a current density as high as 8 A g^{-1}. Such superior electrochemical performance of the electrodes made by directly growing electro-active highly porous Co_3O_4 on a nanostructured $NiSi_x$ conductive current collector makes them very promising for applications in high-performance lithium ion batteries.

1. Introduction

Lithium ion batteries (LIBs) have attracted significant attention as they show great promise as power sources for portable electronic devices because of their high energy density, flexible light weight design and long cycle life.[1–5] Nanostructured transitional metal oxides (MOs, where M is Fe, Co, Ni, and Cu) have been extensively investigated as potential anode materials for LIBs due to their high specific capacity as compared to those of carbon/graphite based materials.[1,2,6–13] Among these MOs, nanostructured Co_3O_4 has been demonstrated as one of the most promising candidates because of its high theoretical specific capacity (890 mA h g^{-1}).[5,14–16] However, due to their poor electrical conductivity and large volume expansion occurring during the cycling process, Co_3O_4 anode materials always suffer from rapid capacity fading, leading to less satisfactory cycling stability.[5,16–19]

One promising avenue to address the aforementioned drawbacks and boost their electrochemical performances is rational design and smart hybridization of nanostructured Co_3O_4 with highly conducting matrices to form novel complex structures.[2,18,20–26] $NiSi_x$ nanowires with high electronic conductivity, which are inactive to Li ions, have been intensively investigated as a good mechanically stable scaffold to form complex core–shell nanowire structures composed of $NiSi_x$ nanowire cores and nanostructured active material shells for LIBs.[27–32] Furthermore, the nanostructured self-standing $NiSi_x$ nanowire collector can be a potential choice to enhance the electrochemical performance of cobalt oxides as promising anodes for LIBs.[32] In this regard, it is supposed to be more promising to achieve smart hybridization of Co_3O_4 nanostructures with $NiSi_x$ nanowires into three-dimensional (3D) heterostructured core–shell nanowire arrays for enhanced electrochemical performances.

To date, various Co_3O_4 nanostructures on bulky conductive substrates, including nickel foam, nickel foil, copper foil and Ti foil, as anodes for LIBs with enhanced electrochemical properties have been demonstrated.[15–17,33–37] Notwithstanding these advances, developing a facile synthetic approach with the characteristics of low growth temperature, simple process and short reaction time without using high pressure to synthesize Co_3O_4 nanostructures, as well as the smart combination of these Co_3O_4 nanostructures with nanostructured current collectors into intriguing architectures to achieve high-performance LIBs is highly desirable but still very challenging and to the best of our knowledge, studies on growing Co_3O_4 nanostructures on a self-standing $NiSi_x$ support have been scarcely reported in the literature.

[a]State Key Laboratory for Physical Chemistry of Solid Surfaces, College of Chemistry and Chemical Engineering, Department of Chemistry, Xiamen University, Xiamen, 361005, PR China. E-mail: yyang@xmu.edu.cn

[b]Department of Mechanical and Biomedical Engineering, City University of Hong Kong, 83 Tat Chee Avenue, Kowloon, Hong Kong, PR China. E-mail: kaizhang@cityu.edu.hk

[c]School of Metallurgy and Environment, Central South University, Changsha, 410083, PR China

† Electronic supplementary information (ESI) available: See DOI: 10.1039/c4ta00967c

‡ These authors contributed equally to this work.

Herein, we first report the synthesis of novel 3D hierarchical heterostructure arrays composed of $NiSi_x$ stems on nickel foam and net-like Co_3O_4 nanosheet branches by advantageously combining the versatility of a facile CVD approach and a simple, yet effective chemical bath deposition (CBD) method at relatively low temperature. The smart combination of Co_3O_4 nanostructures and $NiSi_x$ nanowires on nickel foam holds many merits for LIBs with enhanced performance. Firstly, inactive $NiSi_x$ with excellent mechanical stability connected directly with the current collector (nickel foam) provides a mechanically stable support frame for Co_3O_4 nanostructures, enables fast charge transfer pathways, and avoids the use of polymer binders and conducting additives. Secondly, highly porous Co_3O_4 branches well wrapped on the surface of $NiSi_x$ stems can significantly enhance the effective electrode/electrolyte contact areas together with the amount of electro-active sites and provide a short diffusion path for both electrons and ions. Finally, the novel branched nanoscale heterostructures with lots of free spaces among the branched nanowires can allow for the ease of electrolyte penetration and also accommodate volume expansion during Li^+ uptake/removal. As a result, when used as a binder- and conductive-agent-free anodes for LIBs, the as-synthesized 3D hierarchical $NiSi_x/Co_3O_4$ core–shell heterostructure array electrodes are able to exhibit remarkably enhanced electrochemical performances in terms of high rate capability, large reversible capacity and excellent cycle performance as compared to the Co_3O_4/Ni foam electrode.

2. Experimental section

2.1 Synthesis of $NiSi_x$ nanowires on nickel foam

The self-catalytic $NiSi_x$ nanowires were grown on Ni foam *via* a CVD growth method with SiH_4 diluted in H_2 as a precursor. First, the Ni foam (99.99% purity) with a diameter of 14 mm was ultrasonically cleaned and rinsed with diluted oxalic acid (0.1 vol%) and acetone. The cleaned Ni foam was then transferred into a CVD tube furnace. After that, the $NiSi_x$ nanowires were synthesized by flowing 5 standard cubic centimeter per minute (sccm) SiH_4 and 30 sccm H_2 into the CVD system at the temperature of 570 °C for 60 min.

2.2 Synthesis of hierarchical $NiSi_x/Co_3O_4$ nanowire heterostructure arrays

In a typical procedure, 1.87 g of (0.075 M) cobalt(II) acetate tetrahydrate and 6.79 g of urea (1.132 M) were dissolved in 100 mL of distilled water in a 250 mL Pyrex beaker and stirred to form a clear pink solution. The as-prepared $NiSi_x$ nanowire arrays on Ni foam were immersed into the reaction solution. The backsides of substrates were coated with polyimide tape to prevent the growth of Co_3O_4. The beaker containing the growth solution and substrates was covered with aluminum foil and placed in an oven maintained at 85 °C for 0.5 h to 2 h and then cooled to room temperature naturally. The substrates were then taken out of the solution, rinsed with distilled water and cleaned with alcohol by ultrasonication several times. Finally, the as-fabricated samples were annealed at 300 °C in air for 1.5 h to prepare hierarchical $Co_3O_4/NiSi_x$ nanowire heterostructure arrays. For comparison, Co_3O_4 nanosheets grown directly on nickel foam (Co_3O_4/Ni foam) were synthesized under the same conditions. The morphology, crystalline structure and composition of the as-grown $NiSi_x/Co_3O_4$ core–shell heterostructure arrays were characterized by field emission scanning electron microscopy (Hitachi S4800 FESEM), transmission electron microscopy (FEI Tecnai G2 20 TEM) and X-ray diffraction (RigakuSmartLab XRD).

2.3 Electrochemical measurements of hierarchical $NiSi_x/Co_3O_4$ core–shell nanowire array electrodes

For testing the electrochemical performance, the as-synthesized hierarchical $NiSi_x/Co_3O_4$ core–shell heterostructure arrays grown directly on a nickel foam substrate as the working electrode were dried in a vacuum for 12 h at 120 °C, where the growth time for Co_3O_4 is 2 h. The electrode loading density in this study is 3.25 mg cm^{-2}, containing 80% support frame $NiSi_x$ and 20% active material Co_3O_4. The cells (CR2025) were assembled in a glovebox (Mbraun, LabMaster 100, Germany) under an argon atmosphere by directly using the as-synthesized hierarchical $NiSi_x/Co_3O_4$ core–shell nanowire arrays as the anode. The counter and reference electrodes were lithium metal foil (15 mm diameter), and the electrolyte solution was 1 M $LiPF_6$ (EC : DMC : EMC = 1 : 1 : 1, in volume). The cells were charged and discharged over a voltage range of 0.01–3 V (*versus* Li^+/Li) at room temperature by using a Land CT2001A system (Wuhan, China). Cyclic voltammetry was performed on a CHI608A, scanned from 3.0 to 0.01 V *vs.* Li/Li^+ at a scan rate of 0.1 mV s^{-1}. For impedance measurements, the cells were tested and evaluated. The explored frequency range was from 100 kHz to 10 mHz under AC stimulus with 10 mV of amplitude and no applied voltage bias. Before the EIS measurements, the electrodes were cycled for three cycles, then charged to 3.0 V and kept until the open-circuit voltage was stabilized. On average, the mass loading of the Co_3O_4 nanosheets is about 1.2 mg on a circular disk of Ni foam with a diameter of 14 mm.

3. Results and discussion

Fig. 1 schematically illustrates the synthesis procedure of the 3D hierarchical $NiSi_x/Co_3O_4$ core–shell nanowire arrays on nickel foam by a facile CVD approach in combination with a simple but effective CBD method followed by a calcination process. First, metallic cores of $NiSi_x$ nanowire arrays with a high density are grown vertically on nickel foam by a facile CVD approach. Second, the formation of a branched Co-precursor (cobalt hydroxide carbonate)[38,39] nanosheet shells around the backbone of $NiSi_x$ nanowires is realized by a simple but effective CBD method. Finally, the corresponding Co_3O_4 nanosheets are formed on the surface of $NiSi_x$ nanowires by thermal conversion of the as-prepared Co-precursor (cobalt hydroxide carbonate). The chemical reactions responsible for the formation of Co_3O_4 nanosheets on $NiSi_x$ nanowire surfaces are expressed with the following steps (1–6).[38,39]

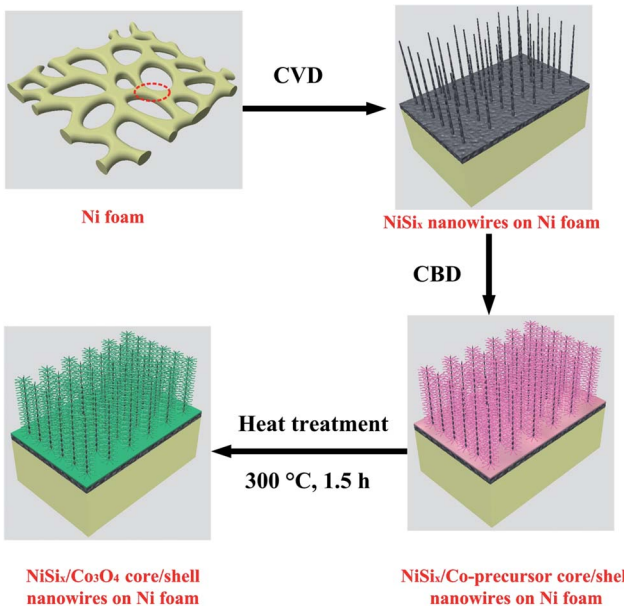

Fig. 1 Schematic illustration of the two-step synthesis of 3D hierarchical $NiSi_x/Co_3O_4$ core–shell nanowire arrays on nickel foam.

$$H_2NCONH_2 + H_2O \rightarrow 2NH_3 + CO_2 \quad (1)$$

$$CO_2 + H_2O \rightarrow CO_3^{2-} + 2H^+ \quad (2)$$

$$NH_3 + H_2O \rightarrow NH_4^+ + OH^- \quad (3)$$

$$Co^{2+} + xOH^- + 0.5CO_3^{2-} + 0.11H_2O \rightarrow Co(OH)_x(CO_3)_{0.5}\cdot 0.11H_2O \quad (4)$$

$$6Co(OH)_x(CO_3)_{0.5}\cdot 0.11H_2O + \left(\frac{5}{2} - \frac{3x}{2}\right)O_2 \rightarrow 2Co_3O_4 + 3CO_2\uparrow + (3x + 0.66)H_2O\uparrow \quad (5)$$

The corresponding representative photographs of the synthesis procedures for $NiSi_x/Co_3O_4$ core–shell nanowire arrays on nickel foam are shown in Fig. S1.†Differential thermal/thermo-gravimetric analysis (DTA-TG) (see ESI, Fig. S2†) is used to characterize the thermal decomposition of the Co-precursor (cobalt hydroxide carbonate). It is clearly observed that a sharp mass loss appears in the temperature range from 100 °C to 300 °C, suggesting the thermal decomposition of the Co-precursor. We therefore selected the temperature of 300 °C for thermal treatment in order to ensure the complete decomposition of the Co-precursor.

Fig. 2 shows the SEM images of the $NiSi_x$ nanowire arrays, Co_3O_4 nanosheets and $NiSi_x/Co_3O_4$ core–shell nanowire arrays on nickel foam. As illustrated in Fig. 2(a), high-density $NiSi_x$ nanowires with lengths up to tens of micrometers are vertically grown on the surface of nickel foam with good uniformity. These nanowires have an average diameter of 20 nm with a very smooth surface (see Fig. 2(b) and S3(a)†). The morphologies of a typical Co_3O_4 nanosheet film grown on a nickel foam substrate are shown in Fig. 2c and d. As shown in Fig. 2(c), the nickel foam

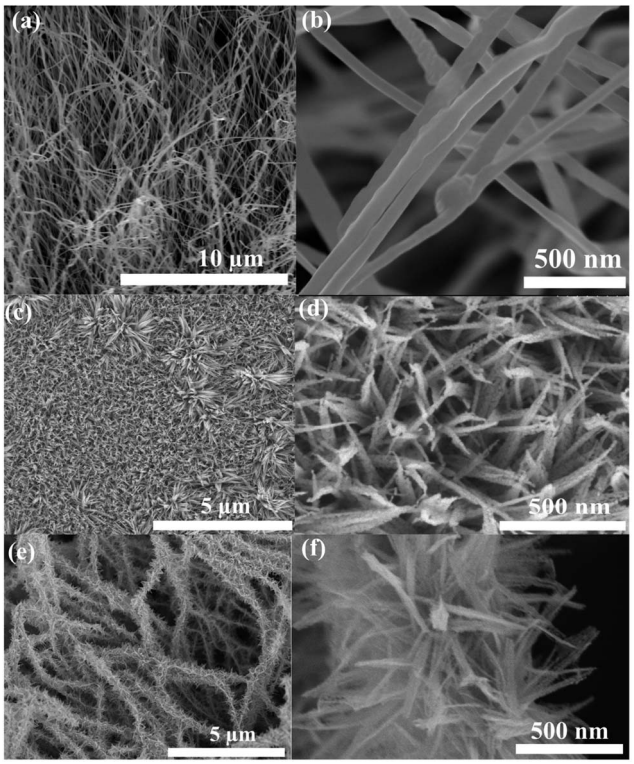

Fig. 2 (a) Low-magnification SEM image of $NiSi_x$ on Ni foam, (b) high-magnification image of $NiSi_x$ on Ni foam, (c) low-magnification SEM image of Co_3O_4 on Ni foam, (d) high-magnification image of Co_3O_4 on Ni foam, (e) low-magnification SEM image of $NiSi_x/Co_3O_4$ core–shell nanowire arrays on Ni foam, and (f) high-magnification image of $NiSi_x/Co_3O_4$ core–shell nanowire array on Ni foam.

skeleton is uniformly covered by many Co_3O_4 nanosheets. These Co_3O_4 nanosheets show a highly porous structure composed of many interconnected small nanograins (Fig. 2(d)). After the integration of Co_3O_4 by CBD, the $NiSi_x$ nanowires become thicker and show a much rougher surface as can be seen in Fig. 2(e). Numerous ultrathin nanosheets of Co_3O_4 grow fairly homogenously along the $NiSi_x$ nanowires arrays, forming 3D core–shell architecture (see Fig. 2(f) and S3(b)†), indicating the intimate interface contact between $NiSi_x$ nanowire cores and branched Co_3O_4 nanosheet shells, which could play the important role of improving the electrochemical performances. These branched Co_3O_4 nanosheet shells are interconnected with each other and fully cover the entire $NiSi_x$ nanowire cores as illustrated in Fig. 2(f) and S3(b).† It is worth noting that the diameter, length and density of the secondary Co_3O_4 nanosheets can be tailored by simply changing the reaction time as shown in Fig. S4† and the as-obtained branched Co_3O_4 nanosheets can be realized on a variety of other nanostructures, such as Si nanowires, CuO nanoneedles, CuO nanoflowers and CuO nanowires (see Fig. S5†). The growth mechanism with respect to the formation of the secondary Co_3O_4 nanosheets could attribute to the "oriented attachment" and "self-assembly" processes.[40,41]

The detailed microstructure of the $NiSi_x$ nanowires and hierarchical $NiSi_x/Co_3O_4$ core–shell nanowires is further

elucidated by TEM and HRTEM. The bare $NiSi_x$ nanowires have a very smooth surface with a diameter of 20 nm and are single-crystalline in nature as shown in Fig. S6.† After the growth of Co_3O_4 for 30 min, the surface of the $NiSi_x$ nanowires is decorated by many ultrathin Co_3O_4 nanoparticles with the thickness of around 20 nm and the structure of the nanowire is still well maintained. The corresponding SAED pattern in Fig. S6(c)† suggests that the $NiSi_x$ nanowire core still maintain its single crystalline structure, indicating that no structural damage is caused by the facile CBD. The HRTEM image of the $NiSi_x$ nanowire edge (see Fig. S6(d)†) provides more evidence that Co_3O_4 nanoparticles are attached to the $NiSi_x$ nanowire surface and the measured *d*-spacings of 0.46 nm and 0.54 nm are consistent with the (111) and (020) lattice planes of the cubic structure Co_3O_4 (PDF 74-2120) and orthorhombic Ni_2Si_3 (PDF89-7167), respectively, which are consistent with the reported results for Co_3O_4 (ref. 16, 17, 35 and 42) and Ni_2Si_3.[43] The typical TEM image of hierarchical $NiSi_x/Co_3O_4$ core–shell nanowires with Co_3O_4 growth of 2 h is shown in Fig. 3. As illustrated in Fig. 3(a), the $NiSi_x$ nanowire core is uniformly wrapped by numerous ultrathin Co_3O_4 nanosheets, which is in accordance with the SEM results. The corresponding SAED pattern of the nanosheet shell taken from the rectangular area marked I in Fig. 3(a) confirms the existence of spinel polycrystalline Co_3O_4. Three typical rings can be readily indexed to the (111), (220), and (311) planes of the cubic Co_3O_4 phase (JCPDS 74-2120). The magnified TEM image shown in Fig. 3(c) of the Co_3O_4 nanosheet shell taken from the rectangular area marked II in Fig. 3(a), clearly demonstrates that the Co_3O_4 nanosheet shells are highly porous composed of nanocrystallites of 5–10 nm in size. The porosity of the Co_3O_4

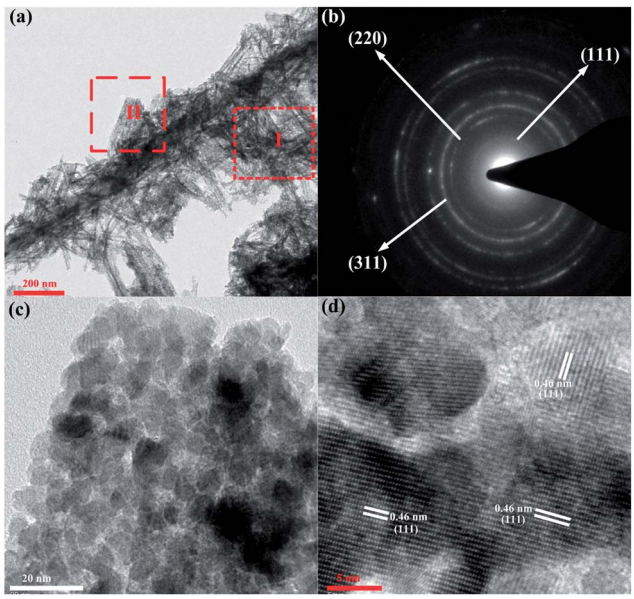

Fig. 3 (a) The low-magnification TEM image of $NiSi_x/Co_3O_4$ core–shell nanowires (b) the SAED pattern of branch Co_3O_4 taken from the rectangular area marked in (a). (c) The enlarged TEM images of branched Co_3O_4 nanosheets (d) high-magnification TEM images of branched Co_3O_4 nanosheets.

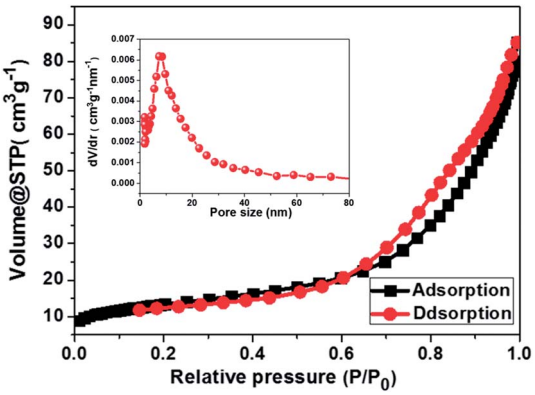

Fig. 4 The N_2 absorption–desorption isotherm of the as-prepared Co_3O_4 nanosheets; the inset is the pore distribution.

nanosheets is characterized by nitrogen isothermal adsorption–desorption measurements. From Fig. 4, a typical IV isotherm with a distinct hysteresis loop in the pressure range of 0.7–1.0 P/P_0 can be clearly observed, suggesting the presence of a mesoporous structure of nanosheets.[44,45] The inset of Fig. 4 shows the pore size distribution of the sample calculated by desorption isotherm *via* the Barret–Joyner–Halenda (BJH) method, which demonstrates that the as-synthesized Co_3O_4 nanosheets possess narrow pore size distribution centered at around 7.7 nm. This result further confirms the mesoporous feature of Co_3O_4 nanosheets. The Brunauer–Emmett–Teller (BET) specific surface area was measured to be 47.2 $m^2\ g^{-1}$.The formation of the mesopores of Co_3O_4 could be attributed to the gas release during the decomposition of the Co-precursor by heat treatment.[44,46,47] This highly porous feature of the Co_3O_4 would allow for the ease of electrolyte penetration, favor the efficient electrode/electrolyte interface contact and also enhance Li^+ and electron diffusion, which is more favorable for the enhancement in electrochemical performances.[48,49] The HRTEM image (Fig. 3(d)) shows clear fringes with a measured interplanar spacing of 0.46 nm, corresponding to the interplanar distance of the (111) plane of cubic Co_3O_4 ($d = 4.67$ Å), in good agreement with the reported results.[16,44] XRD patterns of the as-prepared $NiSi_x$ nanowires, Co_3O_4 nanosheets, and $NiSi_x/Co_3O_4$ core–shell nanowire arrays on nickel foam are shown in Fig. S7.† For the $NiSi_x$ nanowires, except for the three strong peaks and one weak peak coming from the nickel foam and the byproduct of the NiSi phase, respectively, the major diffraction peaks can be indexed to the orthorhombic phase of Ni_3Si_2 (JCPDS 89-7167), which is consistent with the reported results. After the growth of Co_3O_4, three new peaks are observed in addition to the diffraction peaks from the Ni_2Si_3, NiSi and nickel foam. These three peaks are centered at 31.4, 37.1 and 43.9, respectively, which can be indexed respectively to the (220), (331) and (400) planes of the cubic structure of Co_3O_4 (JCPDS 74-2120), suggesting that Co_3O_4 has been successfully assembled on the surface of $NiSi_x$ nanowires.

This 3D core–shell heterostructure is also supported by TEM elemental mapping as shown in Fig. 5. It is observed that the signals of Co and O are strongly detected in the backbone and

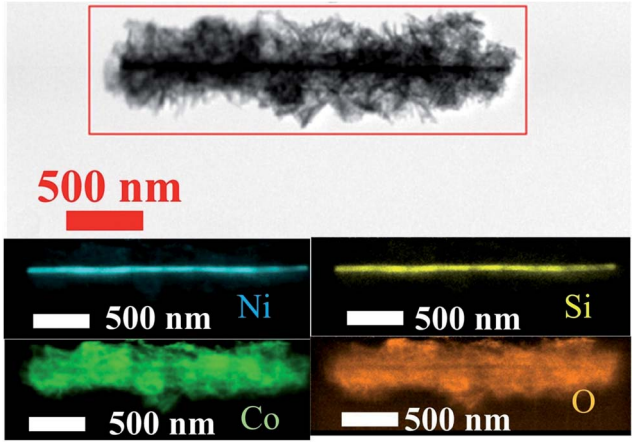

Fig. 5 EDS mapping results of a single hierarchical $NiSi_x/Co_3O_4$ core–shell nanowire.

branch region, while the Ni and Si signals are dominant in the backbone region. According to all these aforementioned results, it is reasonable to assume that branched Co_3O_4 nanosheet shells have been successfully synthesized on the surface of $NiSi_x$ core nanowires. This result is further supported by STEM scan lines shown in Fig. S8.†

Enlightened by the novel 3D hierarchical $NiSi_x/Co_3O_4$ core–shell nanowire array architectures, their lithium storage properties have been investigated when directly used as an integrated binder- and conductive agent-free anode for LIBs. Note that, the capacity contribution of $NiSi_x$ nanowires in LIBs has been proven to be neglected.[27,30] For double check, we tested the bare $NiSi_x$ nanowires on Ni foam under heat treatment at 300 °C for 1.5 h as anodes for LIBs. No apparent potential plateau in the potential range of 0.01 to 3.00 V can be observed (Fig. S9(a)†), indicating that the bare $NiSi_x$ nanowires are electrochemically inactive. Fig. 6(a) shows the CV curves in the first three cycles of the $NiSi_x/Co_3O_4$ core–shell nanowire array electrode with a scan rate of 0.1 mV s^{-1} in the potential range of 0.01–3.0 V. The CV curves are similar to the reported results of Co_3O_4 anodes,[44,48–53] indicating that the $NiSi_x$ core nanowires are indeed electrochemically inactive and just serve as the mechanical support and current collector. In the first cathodic scan, an intense peak located at around 0.72 V can be clearly observed, corresponding to a multi-step electrochemical transition of Co_3O_4 to metallic cobalt.[15,33,48] Then in the first anodic process, one dominant broad oxidative peak at around 2.13 V can be attributed to reversible oxidation of metal Co to cobalt oxide.[44,48] In subsequent cycles, all the redox peaks are found to shift to higher potentials. More interestingly, the subsequent CV curves exhibit good reproducibility with almost the same peak current and integrated area of the cathodic/anodic peak, suggesting high reversibility of lithium storage. The voltage plateau characteristics of the selected discharge–charge profiles measured at a current density of 400 mA g^{-1} are shown in Fig. 6(b). The initial discharge and charge capacities of the as-fabricated $NiSi_x/Co_3O_4$ core–shell nanowire array electrode are 2084 and 1540 mA h g^{-1}, respectively, accounting for a coulombic efficiency of 73.9% as shown in Fig. 6(c). The relatively large irreversible capacity loss in the 1st cycle is likely to be attributed to the electrolyte decomposition and SEI formation, which has been reported by many authors.[15,16,33,48] This phenomenon is also commonly observed in other transition

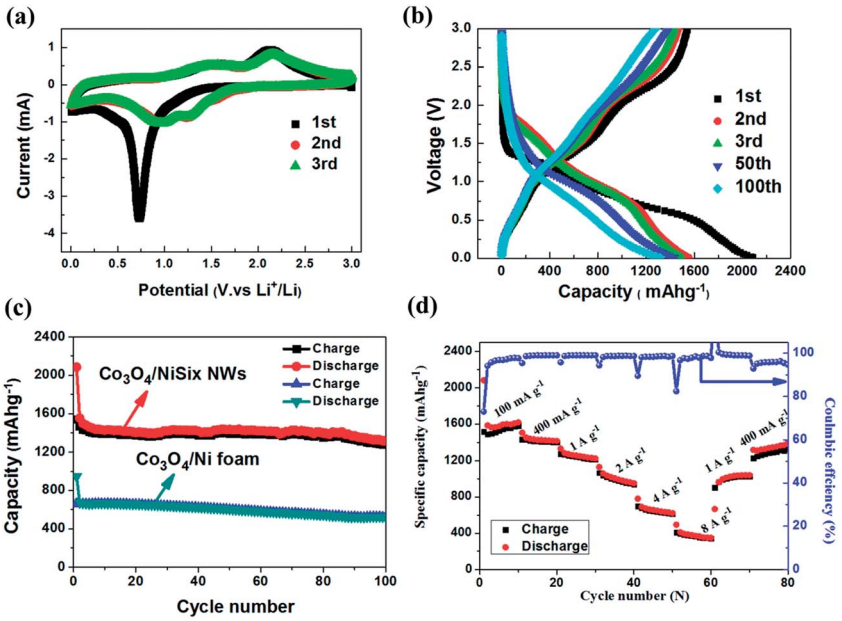

Fig. 6 (a) The first three CV curves of the $NiSi_x/Co_3O_4$ core–shell nanowire array electrode in the potential range of 0.01–3 V at a scan rate of 0.1 mV s^{-1}, (b) selected discharge–charge curves at a current density of 400 mA g^{-1}, (c) cycle performance of the $NiSi_x/Co_3O_4$ core–shell nanowire array electrode and the Co_3O_4/Ni foam electrode at a current density of 400 mA g^{-1}, (d) rate capability of the $NiSi_x/Co_3O_4$ core–shell nanowire array electrode at various current densities.

metal oxide anodes.[47,54,55] Nevertheless, the discharge–charge curve from the 2nd cycle shows good reproducibility and the coulombic efficiency is increased to above 94.6%, suggesting superior cycle performances.

To demonstrate the advantages of hierarchical core–shell nanowire array architectures and $NiSi_x$ nanowire arrays as a good mechanical support and current collector, the electrochemical performances of $NiSi_x/Co_3O_4$ core–shell nanowire arrays on nickel foam and Co_3O_4 directly grown on nickel foam without pre-synthesized $NiSi_x$ nanowires(Co_3O_4/Ni foam, see Fig. 2c and d) are compared. Fig. 6(c) displays the cycle performances of the electrodes made by $NiSi_x/Co_3O_4$ core–shell nanowire arrays and Co_3O_4/Ni foam at a current density of 400 mA g^{-1}. Evidently, the $NiSi_x/Co_3O_4$ core–shell nanowire array electrode exhibits better cycling performance and much higher initial capacity and reversible capacity over 100 cycles than those of the Co_3O_4/Ni foam electrode. From Fig. 6(c), it can be clearly seen that the $NiSi_x/Co_3O_4$ composite electrode delivers an initial capacity of 1540 mA h g^{-1}, while only an initial capacity of 664 mA h g^{-1} is delivered by the Co_3O_4/Ni foam electrode. More remarkably, the $NiSi_x/Co_3O_4$ composite electrode retains a high reversible capacity of 1279 mA h g^{-1} with 83% capacity retention after 100 cycles. In contrast, the Co_3O_4/Ni foam electrode only maintains a reversible capacity of 522 mA h g^{-1} with 79% capacity retention after 100 cycles. The improved electrochemical performances are due to the fact that $NiSi_x$ nanowires on Ni foam as a nanostructured current collector are beneficial in providing an increased surface area compared with that of the bulky Ni foam, which significantly enhances the loading of active materials.[2] Moreover, the $NiSi_x$ nanowires can provide a 1D pathway for electron/ion transport, resulting in a short diffusion length and an enhanced electronic conductivity necessary for higher capacity.[29,30,32] In addition, the synergistic contribution from the $NiSi_x$ nanowires and mesoporous Co_3O_4 nanosheets should be another reason that accounts for their enhanced electrochemical performances. The enhanced performance is even better than the reported results of Co_3O_4 anodes with different morphologies[14,17,44,56] and other metal oxide composite anode materials.[36,57,58]

It is interesting to note that in our case the measured capacities are found to be higher than the theoretical capacity for the bulk Co_3O_4 of 890 mA h g^{-1}. Similar results have also been observed in Co_3O_4 anodes in the literature.[33,42,44,48–50,59–63] For example, Zhan *et al.* showed that the a high reversible capacity of 1450 mA h g^{-1} after 25 cycles at a current density of 50 mA g^{-1} could be retained by porous Co_3O_4 nanosheets.[62] Hu *et al.* demonstrated that a high charge capacity of 1465 mA h g^{-1} after 50 cycles at a current density of 300 mA g^{-1} could be maintained by Co_3O_4 porous nanocages.[49] Xiao *et al.*[48] reported that mesoporous Co_3O_4 hierarchical nanobundles were able to retain a capacity up to 1492.4 mA h g^{-1} even after 100 cycles at a current density of 500 mA g^{-1}. This phenomenon could be associated with the mesoporous feature of Co_3O_4 nanosheets, which can provide extra active sites for Li ion insertion and dramatically facilitate electrolyte penetration as well as effectively increase the amounts of Li^+ transfer, more beneficial for the enhancement of surface Li storage capacities leading to high extra capacity.[33,48,49] In addition, the reversible formation/dissolution of a polymeric gel-like film originating from the decomposition of the electrolyte could deliver an extra capacity *via* a so-called "pseudo-capacitive behavior".[45]

The rate capability of the $NiSi_x/Co_3O_4$ core–shell nanowire array electrode at different current densities is also evaluated as shown in Fig. 6(d). It can be seen that the $NiSi_x/Co_3O_4$ core–shell nanowire array electrode exhibits outstanding rate capability with charge capacities of 1581, 1402, 1212, 937, 612, and 340 mA h g^{-1} after 10 cycles at current densities of 0.1, 0.4, 1, 2, 4, and 8 A g^{-1}, respectively. A capacity higher than 340 mA h g^{-1} even at a current density as high as 8 A g^{-1} is maintained, which is still comparable to that of commercially used graphite. Remarkably, when the high current density is reversed back to low current density, the original high capacity can be regained, indicating the excellent reversibility.

To understand further the advantages of the $NiSi_x/Co_3O_4$ core–shell nanowire array electrode, the as-fabricated $NiSi_x/Co_3O_4$ core–shell nanowire array electrode and the Co_3O_4/Ni foam electrode at open-circuit potential after three cycles are analyzed by EIS. As shown in Fig. 7, the Nyquist plots are composed of one semicircle followed by a slope line. The semicircle represents the charge-transfer impedance of the cell.[32,64] The charge transfer resistances R_{ct} of Co_3O_4/Ni foam (33 Ω) is approximately double that of $NiSi_x/Co_3O_4$ core–shell nanowire arrays (17 Ω), indicating that the use of $NiSi_x$ nanowires on nickel foam as a nanostructured current collector could enable much easier charge transfer at the electrode/electrolyte interface (as compared to Ni foam only) and boost the electronic conductivity.

To investigate the structural stability of the $NiSi_x/Co_3O_4$ core–shell nanowire array electrode during cycling and under different current densities, the morphology of the electrode after cycling and high-rate discharge–charge process is characterized. Fig. 8 shows the SEM images of $NiSi_x/Co_3O_4$ core–shell nanowire array electrodes after discharging–charging for 100 cycles at a current density of 400 mA g^{-1} and 80 discharges–

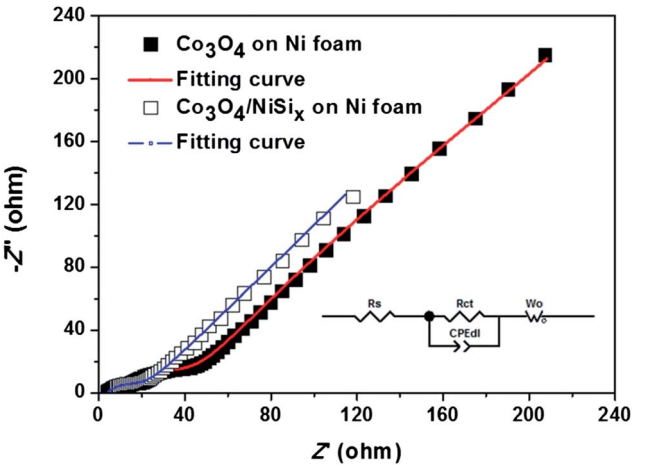

Fig. 7 Nyquist plots of the $NiSi_x/Co_3O_4$ core–shell nanowire array electrode and the Co_3O_4/Ni foam electrode at open-circuit voltage after three cycles.

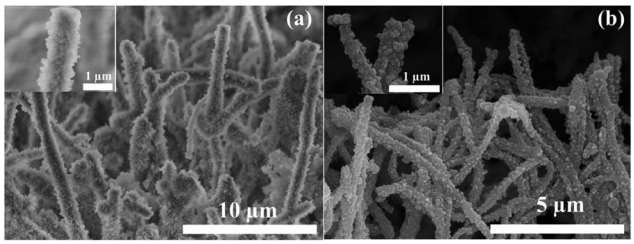

Fig. 8 SEM images of the $NiSi_x/Co_3O_4$ core–shell nanowire arrays: (a) after discharging–charging for 100 cycles at a current density of 400 mA g^{-1} and (b) after the cycling test at various current rates for 80 cycles.

charge cycles at various current rates, respectively. As can be seen, the electrode can still relatively well retain its integrity, except for the increased roughness on the electrode surface and some expansion and merging of branches caused by the redox reactions during the repeated charge–discharge processes, indicating the stable structure of the core–shell architecture.

Based on the aforementioned electrochemical measurements, it is reasonable to conclude that the rational design of integrating active Co_3O_4 branches with the Li inactive $NiSi_x$ nanowires that are directly connected on the current collector could significantly enhance the Li^+ storage capacity and stability of Co_3O_4 materials. The excellent performance of the 3D hierarchical $NiSi_x/Co_3O_4$ core–shell nanowire arrays on nickel foam for being used as the anode for LIBs could be caused by the following aspects. Firstly, the inactive $NiSi_x$ nanowires directly grown on the nickel foam current collector could act as a good mechanical support, and more importantly as an effective conductive pathway for electron transport between the Co_3O_4 materials and the nickel foam current collector.[30] Secondly, the highly porous Co_3O_4 with a high specific surface area greatly facilitates transport of the electrolyte and largely increases the amount of electroactive sites.[41] Finally, the voids among neighboring core–shell nanowire arrays provide sufficient space to buffer the volume change of the $NiSi_x/Co_3O_4$ core–shell nanowire array electrode during lithium insertion–extraction and benefit the structural stability and rate capability.

4. Conclusions

In summary, a novel 3D branched $NiSi_x/Co_3O_4$ heterostructure has been successfully synthesized by a combination of the CVD method and CBD strategy, in which single-crystalline $NiSi_x$ nanowire arrays are primarily grown on nickel foam by a facile CVD approach and then a simple but effective CBD method followed by a heat treatment process induces the growth of branched Co_3O_4 nanosheets around the $NiSi_x$ nanowires. Benefiting from the 3D branched nanowire heterostructure features, the $NiSi_x/Co_3O_4$ core–shell nanowire array electrode has exhibited high capacity together with excellent rate capability and cyclic stability as compared to those of the Co_3O_4/Ni foam electrode. It maintains a high reversible capacity of 1279 mA h g^{-1} over 100 cycles at a current density of 400 mA g^{-1} and a capacity up to 340 mA h g^{-1} after 10 cycles even at a current density as high as 8 A g^{-1}. Considering the outstanding performance and cost-effective large-scale fabrication, we believe that the $NiSi_x/Co_3O_4$ core–shell nanowire arrays grown directly on nickel foam hold great promise as anode materials for advanced high performance lithium ion batteries and may also have wide potential applications in other fields.

Acknowledgements

This work was financially supported by the National Basic Research Program of China (973 program, Grant no. 2011CB935903), the National Natural Science Foundation of China (Grant no. 21233004 and 21021002), and the City University of Hong Kong Seed Grant (Grant no. 7003023).

References

1 L. Ji, Z. Lin, M. Alcoutlabi and X. Zhang, *Energy Environ. Sci.*, 2011, **4**, 2682.
2 J. Jiang, Y. Li, J. Liu, X. Huang, C. Yuan and X. W. Lou, *Adv. Mater.*, 2012, **24**, 5166–5180.
3 P. G. Bruce, B. Scrosati and J. M. Tarascon, *Angew. Chem., Int. Ed.*, 2008, **47**, 2930–2946.
4 C. Wu and Y. Xie, *Energy Environ. Sci.*, 2010, **3**, 1191–1206.
5 M. Armstrong, C. O'Dwyer, W. Macklin and J. Holmes, *Nano Res.*, 2014, **7**, 1–62.
6 M. Reddy, G. S. Rao and B. Chowdari, *Chem. Rev.*, 2013, **113**, 5364–5457.
7 S. Goriparti, E. Miele, F. De Angelis, E. Di Fabrizio, R. Proietti Zaccaria and C. Capiglia, *J. Power Sources*, 2014, **257**, 421–443.
8 H. Wu, J. Chen, H. Hng and X. W. Lou, *Nanoscale*, 2012, **4**, 2526.
9 C. Yuan, H. Wu, Y. Xie and X. W. Lou, *Angew. Chem., Int. Ed.*, 2013, **52**, 2–19.
10 P. Poizot, S. Laruelle, S. Grugeon, L. Dupont and J. M. Tarascon, *Nature*, 2000, **407**, 496–499.
11 Q. Zhang, K. Zhang, D. Xu, G. Yang, H. Huang, F. Nie, C. Liu and S. Yang, *Prog. Mater. Sci.*, 2014, **60**, 208–337.
12 L. Zhang, H. Bin Wu and X. W. Lou, *Adv. Energy Mater.*, 2013, DOI: 10.1002/aenm.201300958.
13 L. Ji and X. Zhang, *Electrochem. Commun.*, 2009, **11**, 795–798.
14 L. Li, K. H. Seng, Z. Chen, Z. Guo and H. K. Liu, *Nanoscale*, 2013, **5**, 1922–1928.
15 L. Wang, B. Liu, S. Ran, H. Huang, X. Wang, B. Liang, D. Chen and G. Shen, *J. Mater. Chem.*, 2012, **22**, 23541.
16 Y. Fu, X. Li, X. Sun, X. Wang, D. Liu and D. He, *J. Mater. Chem.*, 2012, **22**, 17429.
17 Y. Fan, H. Shao, J. Wang, L. Liu, J. Zhang and C. Cao, *Chem. Commun.*, 2011, **47**, 3469–3471.
18 Z. Wu, W. Ren, L. Wen, L. Gao, J. Zhao, Z. Chen, G. Zhou, F. Li and H. Cheng, *ACS Nano*, 2010, **4**, 3187–3194.
19 X. Wang, W. Tian, T. Zhai, C. Zhi, Y. Bando and D. Golberg, *J. Mater. Chem.*, 2012, **22**, 23310.
20 J. Zhu, Y. K. Sharma, Z. Zeng, X. Zhang, M. Srinivasan, S. Mhaisalkar, H. Zhang, H. H. Hng and Q. Yan, *J. Phys. Chem. C*, 2011, **115**, 8400–8406.

21 Y. Wang, F. Yan, S. W. Liu, A. Y. S. Tan, H. Song, X. W. Sun and H. Y. Yang, *J. Mater. Chem. A*, 2013, **1**, 5212.
22 Z. Wu, G. Zhou, L. Yin, W. Ren, F. Li and H. Cheng, *Nano Energy*, 2012, **1**, 107–131.
23 A. Reddy, S. Gowda, M. Shaijumon and P. Ajayan, *Adv. Mater.*, 2012, **24**, 5045–5064.
24 F. Hao, Z. Zhang and L. Yin, *ACS Appl. Mater. Interfaces*, 2013, **5**, 8337–8344.
25 X. Yang, K. Fan, Y. Zhu and J. Shen, *ACS Appl. Mater. Interfaces*, 2013, **5**, 997–1002.
26 L. Li, G. Zhou, X.-Y. Shan, S. Pei, F. Li and H.-M. Cheng, *J. Power Sources*, 2014, **255**, 52–58.
27 K. Kang, K. Song, H. Heo, S. Yoo, G.-S. Kim, G. Lee, Y.-M. Kang and M.-H. Jo, *Chem. Sci.*, 2011, **2**, 1090.
28 N. Du, X. Fan, J. Yu, H. Zhang and D. Yang, *Electrochem. Commun.*, 2011, **13**, 1443–1446.
29 K. Song, S. Yoo, K. Kang, H. Heo, Y.-M. Kang and M.-H. Jo, *J. Power Sources*, 2013, **229**, 229–233.
30 X. Fan, H. Zhang, N. Du, P. Wu, X. Xu, Y. Li and D. Yang, *Nanoscale*, 2012, **4**, 5343–5347.
31 F. Li, H. Yue, P. Wang, Z. Yang, D. Wang, D. Liu, L. Qiao and D. He, *CrystEngComm*, 2013, **15**, 7298.
32 Y. Qi, N. Du, H. Zhang, X. Fan, Y. Yang and D. Yang, *Nanoscale*, 2012, **4**, 991.
33 W. Mei, J. Huang, L. Zhu, Z. Ye, Y. Mai and J. Tu, *J. Mater. Chem.*, 2012, **22**, 9315.
34 J. Chen, X. Xia, J. Tu, Q. Xiong, Y.-X. Yu, X. Wang and C. Gu, *J. Mater. Chem.*, 2012, **22**, 15056.
35 X.-Y. Xue, S. Yuan, L.-L. Xing, Z.-H. Chen, B. He and Y.-J. Chen, *Chem. Commun.*, 2011, **47**, 4718–4720.
36 H. Wu, M. Xu, Y. Wang and G. Zheng, *Nano Res.*, 2013, **6**, 167–173.
37 Y. Li, B. Tan and Y. Wu, *Nano Lett.*, 2008, **8**, 265–270.
38 S. Xiong, J. S. Chen, X. W. Lou and H. C. Zeng, *Adv. Funct. Mater.*, 2012, **22**, 861–871.
39 B. Li, Y. Xie, C. Wu, Z. Li and J. Zhang, *Mater. Chem. Phys.*, 2006, **99**, 479–486.
40 G. Zhang, T. Wang, X. Yu, H. Zhang, H. Duan and B. Lu, *Nano Energy*, 2013, **2**, 586–594.
41 X. Xia, J. Tu, Y. Zhang, X. Wang, C. Gu, X.-B. Zhao and H. J. Fan, *ACS Nano*, 2012, **6**, 5531–5538.
42 N. Du, H. Zhang, B. D. Chen, J. B. Wu, X. Y. Ma, Z. H. Liu, Y. Q. Zhang, D. R. Yang, X. H. Huang and J. P. Tu, *Adv. Mater.*, 2007, **19**, 4505–4509.
43 J. Kim, D. H. Shin, E.-S. Lee, C.-S. Han and Y. C. Park, *Appl. Phys. Lett.*, 2007, **90**, 253103.
44 H. Huang, W. Zhu, X. Tao, Y. Xia, Z. Yu, J. Fang, Y. Gan and W. Zhang, *ACS Appl. Mater. Interfaces*, 2012, **4**, 5974–5980.
45 J. Li, S. Xiong, Y. Liu, Z. Ju and Y. Qian, *ACS Appl. Mater. Interfaces*, 2013, **5**, 981–988.
46 G. Zhang and X. W. Lou, *Adv. Mater.*, 2012, **25**, 976–979.
47 L. Shen, Q. Che, H. Li and X. Zhang, *Adv. Funct. Mater.*, 2013, DOI: 10.1002/adfm.201303138.
48 Y. Xiao, C. Hu and M. Cao, *J. Power Sources*, 2014, **247**, 49–56.
49 L. Hu, N. Yan, Q. Chen and P. Zhang, *Chem.–Eur. J.*, 2012, **18**, 8971–8977.
50 K. T. Nam, D.-W. Kim, P. J. Yoo, C.-Y. Chiang, N. Meethong, P. T. Hammond, Y.-M. Chiang and A. M. Belcher, *Science*, 2006, **312**, 885–888.
51 H. Shim, Y. Jin, S. Seo, S. Lee and D. Kim, *ACS Nano*, 2011, **5**, 443–449.
52 L. Jin, X. Li, H. Ming, H. Wang, Z. Jia, Y. Fu, J. Adkins, Q. Zhou and J. Zheng, *RSC Adv.*, 2014, **4**, 6083.
53 Y. X. Yu, X. Y. Liu, X. H. Xia, Q. Q. Xiong, X. L. Wang, C. D. Gu and J. P. Tu, *Mater. Res. Bull.*, 2014, **51**, 112–118.
54 H. Liu, G. Wang, J. Liu, S. Qiao and H. Ahn, *J. Mater. Chem.*, 2011, **21**, 3046.
55 X. Chen, N. Zhang and K. Sun, *J. Mater. Chem.*, 2012, **22**, 13637.
56 H. Sun, M. Ahmad and J. Zhu, *Electrochim. Acta*, 2013, **89**, 199–205.
57 Q. Q. Xiong, X. H. Xia, J. P. Tu, J. Chen, Y. Q. Zhang, D. Zhou, C. D. Gu and X. L. Wang, *J. Power Sources*, 2013, **240**, 344–350.
58 Q. Xiong, J. Tu, X. Xia, X. Zhao, C. Gu and X. Wang, *Nanoscale*, 2013, **5**, 7906–7912.
59 X. Rui, H. Tan, D. Sim, W. Liu and C. Xu, *J. Power Sources*, 2012, **222**, 97–102.
60 J. Wang, N. Yang, H. Tang, Z. Dong, Q. Jin, M. Yang, D. Kisailus, H. Zhao, Z. Tang and D. Wang, *Angew. Chem., Int. Ed.*, 2013, **125**, 6545–6548.
61 A. Pan, Y. Wang, W. Xu, Z. Nie, S. Liang, Z. Nie, C. Wang, G. Cao and J. Zhang, *J. Power Sources*, 2014, **255**, 125–129.
62 F. Zhan, B. Geng and Y. Guo, *Chem.–Eur. J.*, 2009, **15**, 6169–6174.
63 L. Tian, H. Zou, J. Fu, X. Yang, Y. Wang, H. Guo, X. Fu, C. Liang, M. Wu, P. K. Shen and Q. Gao, *Adv. Funct. Mater.*, 2010, **20**, 617–623.
64 J. Liu, C. Liu, Y. Wan, W. Liu, Z. Ma, S. Ji, J. Wang, Y. Zhou, P. Hodgson and Y. Li, *CrystEngComm*, 2013, **15**, 1578–1585.

